$K\alpha$ satellite transitions in elements with $12 \leqslant Z \leqslant 30$ produced by electron incidence

Silvina P. Limandri,[1,2] Rita D. Bonetto,[3,4] Alejo C. Carreras,[1,2] and Jorge C. Trincavelli[1,2]

[1]*Instituto de Física Enrique Gaviola, Consejo Nacional de Investigaciones Científicas y Técnicas, Argentina*
[2]*Facultad de Matemática, Astronomía y Física, Universidad Nacional de Córdoba, Córdoba, Argentina*
[3]*Centro de Investigación y Desarrollo en Ciencias Aplicadas Dr. Jorge Ronco (CINDECA), Consejo Nacional de Investigaciones Científicas y Técnicas, Argentina*
[4]*Facultad de Ciencias Exactas, Facultad de Ingeniería, Universidad Nacional de La Plata, La Plata, Argentina*

The emission of x-ray satellite lines in the $K\alpha$ region of Mg, Si, Sc, Ti, Cr, Fe, Ni, and Zn induced by electron incidence was studied by means of wavelength dispersive spectroscopy. The satellite lines studied were $K\alpha'$, $K\alpha_3$, $K\alpha_4$, $K\alpha_5$, $K\alpha_6$, and two transitions denoted here as $K\alpha_{22}$ and $K\alpha_{12}$. Energy shifts with respect to the main $K\alpha_1$ diagram line and transition probabilities relative to the whole $K\alpha$ group were determined for a number of lines through a careful spectral processing. The dependence of these parameters, as well as of the $K\beta$:$K\alpha$ intensity ratio, on the atomic number was compared with previous experimental and theoretical determinations when available. A discussion about the different mechanisms responsible for vacancy creation involved in the production of double-ionization satellites was performed in the light of the results obtained. Finally, the behavior of the satellite intensities as a function of the incidence energy was discussed for silicon.

PACS number(s): 32.30.Rj, 32.70.Fw, 33.70.Jg, 34.80.Dp

I. INTRODUCTION

Single K vacancy production by electron impact is well understood within the framework of a single-vacancy picture. This process leads to the emission of x rays and Auger electrons. The characteristic x rays emitted from atoms having initially one inner-shell vacancy which is filled by a full radiative process are called the diagram lines. The x-ray lines arising out of multiply ionized atoms associated to the $K\alpha$ or $K\beta$ diagram lines are termed the high-energy K satellites, $K\alpha L^n$ or $K\beta M^n$, where n is the initial number of holes in the L or M shell. Apart from this type of satellite line, there is another effect that produces satellite bands: the radiative Auger effect (RAE). In this process, instead of the initial K hole being filled along with the emission of either a full-energy $K\alpha$ or $K\beta$ photon or a full-energy Auger electron, there is simultaneous emission of a lower-energy photon and excitation of an outer-shell electron. The RAE processes compete with the characteristic $K\alpha$ or $K\beta$ x-ray emission processes and produce a broad structure with energy less than the corresponding diagram line. The maximum of this continuous energy distribution is known as the RAE edge, and it corresponds to an electron emitted with zero kinetic energy. On the other hand, the K hypersatellite transitions occur in doubly K-shell ionized atoms, with or without simultaneous ionization of outer shells.

The study of the satellite lines is of great interest, since they provide information on intra-atomic electron correlation, excitation dynamics, relaxation, and other effects that influence the x-ray emission process. Regarding $K\alpha$ transitions, several works were carried out to investigate satellite emissions induced by photon [1–16], proton [17–20], heavy-ion [17,21,22], and electron [13,23–29] impact, although most of them were focused on a few particular elements or transitions. Some theoretical studies related to $K\alpha$ satellite transitions were also performed [13,30–36]. Nevertheless, the results obtained by these authors present significant discrepancies, and data about some elements are scarce or not available for electron incidence.

After an exhaustive study of the $K\beta$ satellite lines in the range of elements with $12 \leqslant Z \leqslant 30$ published in a previous paper [37], a study of the $K\alpha$ satellite transitions for the same range of elements is presented in this work. The x-ray emission was induced by electron incidence and detected by a wavelength dispersive spectrometer. The measured spectra were processed by means of a software package based on a parameter refinement method described previously [38]. A careful treatment was carried out for spectral deconvolution, involving the use of Voigt functions to describe the peak shape, because they combine properly the Lorentzian natural profile with the Gaussian instrumental broadening [37].

The satellite transitions studied in this work are, in order of increasing energy: two lines distorting the main diagram peaks ($K\alpha_1$ and $K\alpha_2$) denoted here as $K\alpha_{22}$ and $K\alpha_{12}$, the $K\alpha'$ transition located at the high-energy side of the $K\alpha_1$ peak, and the $K\alpha_3$, $K\alpha_4$, $K\alpha_5$, and $K\alpha_6$ lines.

The lines closest to the main peaks are $K\alpha_{22}$ and $K\alpha_{12}$, located at the low-energy side of $K\alpha_2$ and between $K\alpha_2$ and $K\alpha_1$, respectively. These satellite lines can be attributed to the distortion of the energy levels produced by one $3d$ spectator hole [13,16,29], i.e., they would be $K\alpha M^1$ transitions, according to this picture. Another possible explanation is based on RAE KLM processes, for which the initial K-shell vacancy is filled by an L electron, and the energy balance is achieved by the joint emission of an x-ray photon and an M electron [28,39,40].

The $K\alpha'$, $K\alpha_3$, and $K\alpha_4$ satellite lines arise from transitions that occur in the presence of a $2p$ spectator hole ($K\alpha L^1$ transitions) [2], and the $K\alpha_5$ and $K\alpha_6$ transitions involve triple ionizations with two $2p$ spectator holes ($K\alpha L^2$ transitions) [41]. Four mechanisms lead to the production of spectator holes: shake-off, shake-up, two-step one (TS1), and two-step two (TS2) [37]. The probability of the first two mechanisms is independent of the incident particle, whereas for the other

TABLE I. Experimental conditions.

Element	Incidence energy E_o (keV)	Crystal (plane)	Collimator slit size (mm)
Mg	18	TAP (101)	2.5
Si	3–6–9–12–15–18	PET (002)	2.5–2.5–2.5–2.5–2.5–0.9
Sc, Ti	21	PET (002)	0.02
Cr, Fe, Ni, Zn	21	LiF (200)	0.02

two, it depends on the energy and kind of projectile. The last two processes are referred to as two-step mechanisms. In TS1 the electron ejected after the first collision interacts with another bound electron of the same atom creating a new vacancy. On the other hand, TS2 refers to a process in which both vacancies are generated sequentially by the same incident particle; therefore, these processes cannot take place by photon incidence. Therefore, the comparison of relative intensities of spectator-hole satellite lines induced by incident particles of different kinds and energies can shed light on some ionization mechanisms.

The Z dependence of the energy shifts and relative intensities of the considered satellite lines was studied and compared with experimental and theoretical results available in the literature. In addition, the dependence of the $K\alpha L^1$ and $K\alpha L^2$ transition probabilities on the incidence energy E_o was investigated for silicon.

II. EXPERIMENT

$K\alpha$ x-ray spectra were measured for elements with $12 \leqslant Z \leqslant 30$ by means of a LEO 1450 VP scanning electron microscope (SEM) equipped with an INCA WAVE 700 wavelength dispersive spectrometer (WDS) from the Laboratorio de Microscopía Electrónica y Microanálisis (LABMEM) of the Universidad Nacional de San Luis, Argentina. The arrangement of the WDS is Johansson type for the thallium acid phthalate (TAP), pentaerythritol (PET), and LiF analyzer crystals used. The spectra were collected from pure standards with an incident beam current around 110 nA and a take-off angle of $29°$. The other experimental conditions are summarized in Table I. The only element measured at different incidence energies was Si, in order to study the dependence of the satellite emission on the overvoltage $U_o = E_o : E_c$, where E_c is the K-shell ionization energy in the case of single ionization, or the sum of the ionization energies of the involved atomic shells in the case of multiple ionization.

The spectral fitting was performed by means of the optimization routine implemented in the software POEMA, developed previously [42,43]. This method consists in minimizing the differences between the experimental spectrum and an analytical function proposed to describe it, which takes into account characteristic peaks, bremsstrahlung emission, and detection artifacts. The intensities of the characteristic lines were evaluated by considering the so-called ZAF (atomic number, absorption, and fluorescence) corrections, with line profiles given by Voigt functions [44]. An empirical model was used to describe the bremsstrahlung contribution [45]. The spectra were corrected by the detection efficiency of the spectrometer using a model developed previously [46]. A more

detailed description of the methodology used for the spectral processing was given in a recent paper [38].

III. RESULTS AND DISCUSSION

In Fig. 1, experimental $K\alpha$ spectra of magnesium, silicon, chromium, and nickel are presented as examples along with their respective fits. As can be seen, the main peaks as well as the weak satellite lines are properly described by means of the spectral processing method mentioned. These four examples present the main spectral features observed in all the elements studied. Details about these features will be described below. The line energies and transition probabilities relative to the whole $K\alpha$ group obtained through the spectral processing are summarized in Tables II–IV.

The natural linewidths of the $K\alpha_1$ and $K\alpha_2$ diagram lines were taken from Campbell and Papp [47], for all the elements studied, and the characteristic energies of these two lines were taken from Bearden [48], except for silicon. In this case, the energy of the $K\alpha_2$ line was determined from the spectral analysis and the value obtained, $1.739\,62 \pm 0.000\,01$ keV, is close to the datum published by Bearden, $1.739\,38 \pm 0.000\,04$ keV. In the case of magnesium, the $K\alpha_1$ and $K\alpha_2$ lines were considered as a doublet $K\alpha_{1,2}$ at 1.2536 keV, according to Bearden [see Fig. 1(a)]. For the other elements, the presence of the $K\alpha_{12}$ peak between the diagram lines [see, for example, Figs. 1(c) and 1(d)], and the resolution of the spectrometer in the corresponding energy range complicate the fitting process and prevent the determination of the $K\alpha_2$ energy. Regarding the satellite lines, all the involved parameters, i.e., characteristic energies, relative intensities, and peak widths, were obtained here as a result of the spectral processing. The natural linewidths are not reported, because their values are masked by the experimental broadening.

The uncertainties of the results obtained were estimated by error propagation from the uncertainties of the intensities registered for each channel i, which were regarded as stochastic variables, with mean values y_i and standard deviations given by $\sigma(y_i) = \sqrt{y_i}$. A detailed description of the method for error estimation was given previously [43].

Notice that the relative intensities resulting from the spectral processing are very sensitive to the analytical function used to describe the line profiles, particularly for strongly overlapped peaks. To get a more realistic description of the spectra, the relative intensity R_1 for the diagram and satellite lines associated to $L_3 \rightarrow K$ transitions ($K\alpha_1$ group) was constrained to satisfy the theoretical ratio R_1^{theor}, proposed by Scofield [49] for single ionization. Actually, part of the counts corresponding to the diagram lines is shared among the satellite lines when multiple ionization is taken into account. Assuming that, in
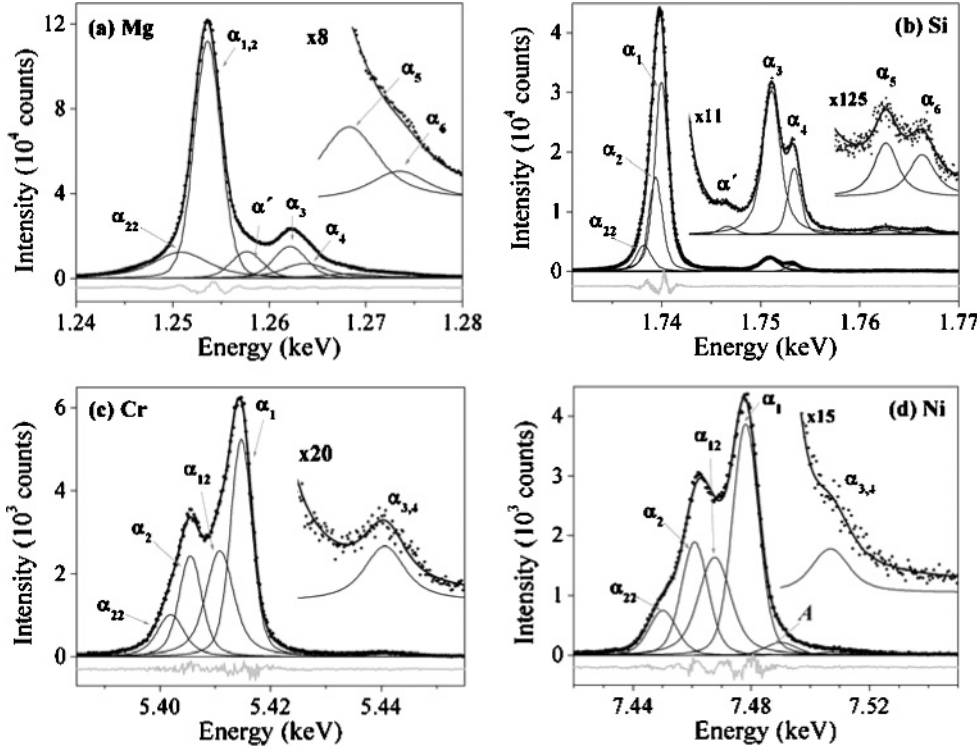
FIG. 1. (a) Magnesium, (b) silicon, (c) chromium, and (d) nickel $K\alpha$ spectra. Dots: measured spectra; black thick solid line: analytical spectra; gray line: differences between experimental and analytical spectra. The satellite transitions are indicated with thin black solid lines. The insets show amplified views of spectral regions that include weak peaks.

a first approximation, the probability of a particular decay (from L_2 or L_3) to the K shell is unaffected by any slight distortion of the atomic energy levels produced by spectator holes, then the intensity fraction of the satellite lines coming from each of the diagram lines satisfies the theoretical ratio based on a single-vacancy picture. Thus, the contribution of the satellite lines to the $K\alpha_1$ group is given by the product $R_1^{\text{theor}} R_{\text{sat}}^{\text{expt}}$, where $R_{\text{sat}}^{\text{expt}}$ is the relative intensity of all the satellite transitions. Taking this fact into account, the relative intensity R_1 associated with the $K\alpha_1$ group was obtained by

$$R_1 = R_1^{\text{expt}} + R_1^{\text{theor}} R_{\text{sat}}^{\text{expt}},$$

where R_1^{expt} is the relative intensity measured for the $K\alpha_1$ diagram line. The constraint imposes the condition $R_1 = R_1^{\text{theor}}$, which was applied iteratively in subsequent fits of the spectra to obtain the particular relative intensities for the

diagram and satellite lines. The same criterion was applied to the $K\alpha_2$ group.

All the satellite lines associated with $2p$ spectator-hole transitions exhibit a similar behavior as a function of the atomic number: the energy shift with respect to the $K\alpha_1$ line increases, while the relative intensity decreases, as can be observed in Figs. 3–5. Some particular remarks related to each kind of transition will be discussed in the following subsections.

A. $K\alpha_{22}$ and $K\alpha_{12}$ lines

These two lines were found in the Cr, Fe, Ni, and Zn spectra [see, for example, Figs. 1(c) and 1(d)], which were measured with the LiF crystal. The lower resolution of the PET crystal in the Sc-$K\alpha$ and Ti-$K\alpha$ energy regions complicate the deconvolution of these groups, and $K\alpha_{22}$ and $K\alpha_{12}$ lines have not been observed for these elements. In addition, for Mg and Si, only the $K\alpha_{22}$ line was studied, since the main $K\alpha_1$ and

TABLE II. Energies (E) and transition probabilities relative to the $K\alpha$ group (RTP) for Mg, Si, and Sc. Numbers in parentheses are the estimated uncertainties in the last digit.

	Mg		Si		Sc	
Transition	E (keV)	RTP	E (keV)	RTP	E (keV)	RTP
$K\alpha_{22}$	1.2508(2)	0.163(8)	1.738 64(7)	0.178(7)		
$K\alpha_2$			1.739 62(1)	0.250(4)	4.0861[a]	0.330(2)
$K\alpha_1$	1.2536[a]	0.554(4)	1.739 98[a]	0.495(7)	4.0906[a]	0.650(2)
$K\alpha'$	1.257 66(8)	0.075(7)	1.7464(2)	0.0017(3)		
$K\alpha_3$	1.2622(1)	0.10(2)	1.750 91(3)	0.0547(9)	4.110(2)	0.008(4)
$K\alpha_4$	1.2637(6)	0.07(3)	1.753 22(2)	0.0170(9)	4.1156(4)	0.012(4)
$K\alpha_5$	1.2682(4)	0.028(8)	1.7627(2)	0.0022(4)		
$K\alpha_6$	1.2734(4)	0.012(4)	1.7663(3)	0.0022(5)		

[a]Characteristic energies taken from Bearden [48].

TABLE III. Energies (E) and transition probabilities relative to the $K\alpha$ group (RTP) for Ti, Cr, and Fe. Numbers in parentheses are the estimated uncertainties in the last digit.

Transition	Ti		Cr		Fe	
	E (keV)	RTP	E (keV)	RTP	E(keV)	RTP
$K\alpha_{22}$			5.4019(3)	0.106(7)	6.384(3)	0.08(4)
$K\alpha_2$	4.5049[a]	0.331(2)	5.405 51[a]	0.203(4)	6.390 84[a]	0.21(3)
$K\alpha_{12}$			5.410 82(7)	0.283(7)	6.3970(2)	0.305(6)
$K\alpha_1$	4.5108[a]	0.651(2)	5.414 72[a]	0.398(3)	6.403 84[a]	0.402(6)
$K\alpha_{3,4}$	4.5347(2)	0.0185(6)	5.4406(3)	0.0114(6)	6.4327(6)	0.0067(8)

[a]Characteristic energies taken from Bearden [48].

$K\alpha_2$ diagram lines are very close, and a good fit was achieved with no need for an additional peak [see Figs. 1(a) and 1(b)].

The origin of these structures has been attributed to *KLM* radiative Auger processes [28,39,40,50] and to $3d$ spectator-hole transitions [6,13,16,29,51]. The intensities resulting from the spectral processing are very sensitive to the analytical function used to describe the line profiles. For instance, if a Lorentzian profile is used for the main diagram lines, the intensities of the $K\alpha_{22}$ and $K\alpha_{12}$ lines are noticeably underestimated, since this function decays more slowly than the more realistic Voigt function used here.

According to results reported by Hölzer *et al.* [6], the $K\alpha_{22}$ ($K\alpha_{21}$) line moves around 1.4 (1.7) eV toward the low-energy side of the main $K\alpha_2$ ($K\alpha_1$) line for elements with $24 \leqslant Z \leqslant 30$. These shifts do not exhibit any clear trend with the atomic number. The $K\alpha_{22}$ and $K\alpha_{12}$ energy shifts found here are greater for this range of elements (see Tables III and IV), and they show an increasing trend with Z similar to the behavior found for the other satellite transitions. Nevertheless, the corresponding intensities are quite similar to that published by Hölzer *et al.* and other authors [16,52], as can be seen in Fig. 2.

The experimental results shown here are, for $3d$ transition elements, above the theoretical calculations of the joint electron shake probabilities from all the atomic levels higher than $2p$ [53]. In Fig. 2, these joint probabilities are also plotted for comparison. These theoretical results exclude the $2p$ shake probabilities because they originate the $K\alpha_{3,4}$ lines, which were considered separately. On the other hand, $2s$ shake probabilities are negligible, while $1s$ shake processes lead

to hypersatellite lines, and then they were not considered here. That is to say, even taking into account the relevant shake contributions, the theoretical predictions are below the experimental results in the range of atomic numbers between 20 and 30. The energy spread of the corresponding multiplet arising from the electronic structure of the atoms in this range, which have a partly or fully populated $4s$ shell and an open $3d$ shell [16], could produce a redistribution of the diagram line emissions in a wider energy range. Thus, part of the $K\alpha_{12}$ and $K\alpha_{22}$ lines, not taken into account by shake processes, would be related to the energy spread of the multiplet. On the other hand, the radiative Auger effect could also contribute to the $K\alpha_{12}$ and $K\alpha_{22}$ lines, but to a smaller extent, since the *KLM* Auger emission rates are lower than 1% of the radiative transition rate corresponding to the $K\alpha$ diagram lines [49].

The shoulder present at the low-energy side of the Ni and Zn spectra, corresponding to the $K\alpha_{22}$ line can be clearly seen at energies shifted more than 10 eV from the main $K\alpha_2$ peak [see Fig. 1(d) for nickel]. The spectra measured by Hölzer *et al.* [6], with a better energy resolution, do not present this structure at those energies. The reason for this discrepancy is still unclear, but it may be due to a possible dependence of the transition $K\alpha_{22}$ on the excitation energy, since the overvoltage
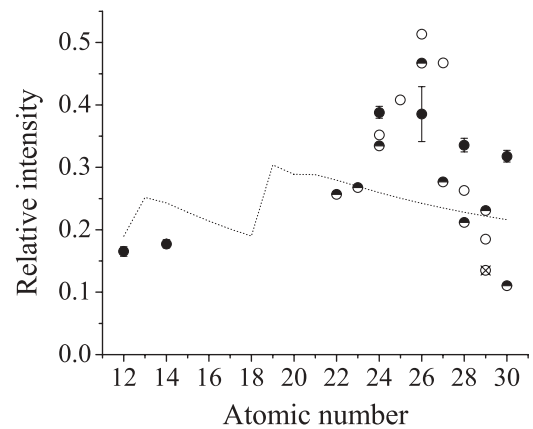
TABLE IV. Energies (E) and transition probabilities relative to the $K\alpha$ group (RTP) for Ni and Zn. Numbers in parentheses are the estimated uncertainties in the last digit.

Transition	Ni		Zn	
	E (keV)	RTP	E (keV)	RTP
$K\alpha_{22}$	7.4501(4)	0.089(5)	8.5987(4)	0.064(3)
$K\alpha_2$	7.460 89[a]	0.213(7)	8.615 78[a]	0.193(5)
$K\alpha_{12}$	7.4677(4)	0.247(9)	8.6234(3)	0.254(9)
$K\alpha_1$	7.478 15[a]	0.415(9)	8.638 86[a]	0.375(7)
A[b]	7.4901(9)	0.028(6)	8.6555(6)	0.11(1)
$K\alpha_{3,4}$	7.507(2)	0.009(3)	8.680(3)	0.009(8)

[a]Characteristic energies taken from Bearden [48].
[b]Peak of unknown origin (see Sec. III B).

FIG. 2. Intensity ratios $K\alpha_{22}$:$K\alpha$, for $Z = 12$ and 14, and $(K\alpha_{22} + K\alpha_{12})$:$K\alpha$ for $Z = 22$–30 as a function of the atomic number. Filled circles: present results; open circles: [6]; crossed circle: [52]; half-filled circles: [16]. Finally, the dotted line represents theoretical results for the electron shake probabilities from the most external shells, according to Ref. [53].
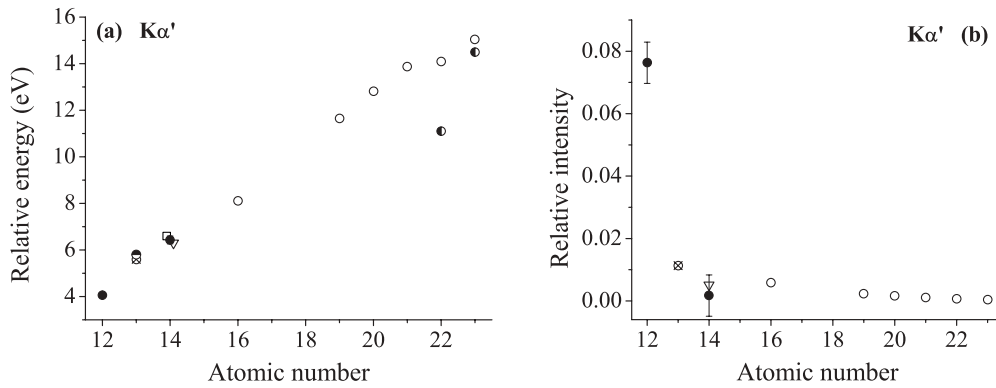
FIG. 3. Parameters related to the $K\alpha'$ line as functions of the atomic number. The point shape indicates the excitation source: electrons (circles), photons (triangles), and protons (squares). Filled circles: present results; open circles: [24]; half-filled circles: [29] ($Z = 12$) and [27] ($Z = 22$ and 23); crossed circles: [25]; open triangles: [2]; open squares: [19]. (a) Energy shift with respect to the $K\alpha_1$ line. (b) Intensity relative to the $K\alpha$ group.

used by Hölzer *et al.* [6] is around 3.6, whereas it is around 2.5 in the present study.

B. $K\alpha'$ line

This transition was observed only for Mg and Si (the elements with the lowest Z in the range studied). Although a shoulder was found at the high-energy side of the main $K\alpha_1$ peak for Ni and Zn [the "A" peak in Fig. 1(d)], neither its position nor its relative intensity follow the trend with the atomic number reported by other authors for the $K\alpha'$ line [7,24,27], so this structure is subject to further investigation. According to the results available in the literature, the energy of the $K\alpha'$ line relative to the $K\alpha_1$ line exhibits a linearly increasing behavior with the atomic number. Even when the present results correspond only to the low-Z region, they follow the general trend [see Fig. 3(a)].

Regarding the intensity of this transition relative to the $K\alpha$ group, the present value for Si also seems to follow the general behavior [see Fig. 3(b)]. The datum for Mg, instead, seems to be above the general trend, although the lack of data in this Z region prevents us from performing a reliable comparison. Notice that, in the spectrum of Mg, the $K\alpha'$ line presents a strong overlapping with the $K\alpha_{1,2}$ doublet [see Fig. 1(a)], whereas for Si, these lines are clearly separated [Fig. 1(b)], which makes the intensity obtained more reliable.

C. $K\alpha_3$ and $K\alpha_4$ lines

These transitions were observed for all the elements studied, although they were considered as a doublet for Ti, Cr, Fe, Ni, and Zn. Relative intensities and energies as functions of the atomic number are plotted in Fig. 4, along with other theoretical and experimental data. For Mg, Si, and Sc, the energy of the $K\alpha_{3,4}$ group was determined by taking the
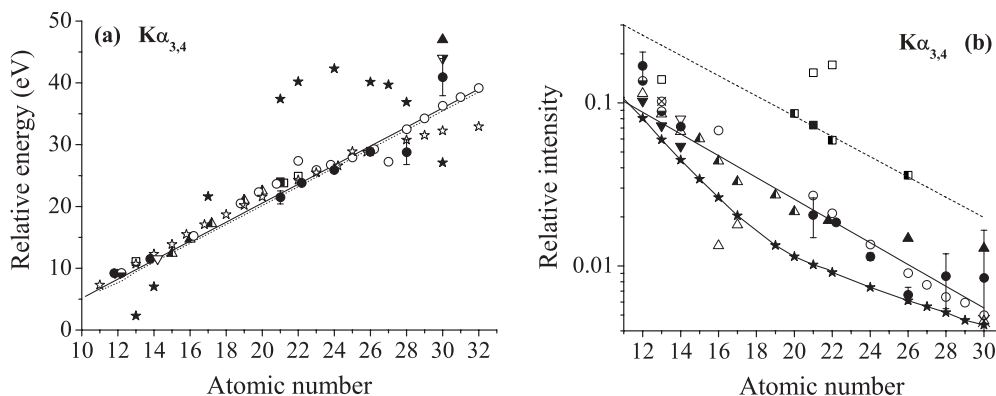

FIG. 4. Parameters related to the $K\alpha_{3,4}$ group as functions of the atomic number. The point shape indicates the excitation source: electrons (circles); photons (triangles); protons and heavy ions (squares). (a) Energy shift with respect to the $K\alpha_1$ line. Filled circles: present results; open circles: [24]; half-filled circles: [54]; filled up triangles: Ref. [9]; half-filled up triangles: [4]; open triangles: [2]; half-filled down triangles: [11]; filled squares: [17]; open squares: [21]. Theoretical results given in [36] (filled stars) and [34] (open stars), and data compiled in [55] (dashed line) are also plotted. The solid line is a linear fit to our results. (b) Intensity relative to the $K\alpha$ group. Filled circles: present results; open circles: [24]; crossed circles: [25]; half-filled circles: [54]; filled up triangles: [9]; half-filled up triangles: [4]; filled down triangles: [10]; crossed triangles: [1]; open up triangles: [14]; open down triangles: [2]; filled squares: [17]; open squares: [21]; half-filled squares: [18]. The solid line is a linear fit to the data obtained by electron and photon incidence; whereas the dashed line is a linear fit to the data obtained by proton incidence. Finally, the line with stars represents the theoretical results from [53].
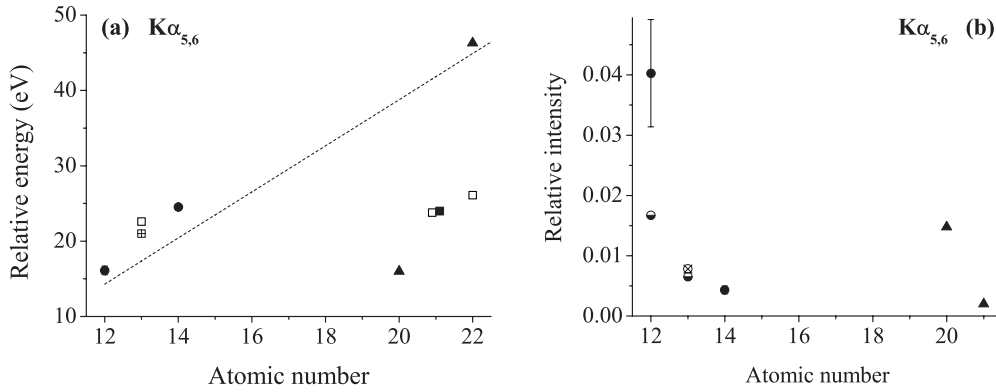
FIG. 5. Parameters related to the $K\alpha_{5,6}$ group as functions of the atomic number. The point shape indicates the excitation source: electrons (circles); photons (triangles); protons and heavy ions (squares). (a) Energy shift with respect to the $K\alpha_1$ line. Filled circles: present results; filled triangles: [9]; filled squares: [17]; open squares: [21]; crossed squares: [56]. Data compiled in [55] (dashed line) are also plotted. (b) Intensity relative to the $K\alpha$ group. Filled circles: present results; crossed circles: [25]; half filled circles: [55]; filled triangles: [9].

intensity-weighted average of the $K\alpha_3$ and $K\alpha_4$ energies, while the corresponding intensity was calculated as the sum of the $K\alpha_3$ and $K\alpha_4$ intensities. The same procedure was carried out with the data published by those authors which have treated both peaks separately, in order to perform the comparison of all the results.

As can be seen from Fig. 4(a), the linear increase of the energy shift is in good agreement with theoretical and experimental results obtained by other authors using diverse excitation sources. This agreement is expected, since the distortion of the atomic levels depends on the vacancy shell but not on the process which originates that vacancy. $K\alpha_{3,4}$ relative intensities also agree with the available results obtained by electron and photon incidence, although they are different from the data determined by other excitation sources.

The relative intensities are related to the probability of multiple-vacancy production, which increases with the mass and charge of the incident particle. Among the mechanisms that produce multiple vacancies, mentioned in the Introduction, are shake-up, shake-off, TS1, and TS2, the latter can occur only for charged particles and its probability depends on the projectile. The probabilities of shake-up and shake-off are, instead, independent of the excitation source; and, according to theoretical calculations [53], they decrease with the atomic number. The good agreement between the results obtained by electron and photon excitation shown in Fig. 4(b) suggests that TS2 processes are not the dominant mechanisms of multiple-vacancy creation for the overvoltages considered. From the comparison between theoretical calculations for the shake probabilities [53] and the experimental intensities for electron and photon excitation, it can be concluded that even when these processes are main contributors to vacancy creation, the two-step mechanisms must also be considered. Since the TS2 effect cannot take place with photon incidence, TS1 is the only additional mechanism responsible for the emission of the $K\alpha_{3,4}$ group.

All the experimental intensities shown in Fig. 4(b) exhibit an exponential decrease with Z, except for the results obtained by heavy-ion incidence [21]. Moreover, the intensities obtained by electron and proton impact decrease with the same slope, in a logarithmic scale. In other words, the ratio between

the probability of double-vacancy creation by protons and by electrons is the same for all the elements studied here, taking a value around 1.5. The few data available for heavy-ion incidence show a different dependence on Z, which suggests that other processes are involved in the creation of spectator holes.

D. $K\alpha_5$ and $K\alpha_6$ lines

These transitions were observed only for Mg and Si. The energies and relative intensities obtained can be seen in Table II and Fig. 5. In this figure, both lines were grouped in a doublet, as in the case of $K\alpha_3$ and $K\alpha_4$ lines, for comparison. Similar to the other spectator-hole satellite lines studied, the energy shift increases, and the relative intensity decreases with the atomic number. It can be seen that our data for energy shifts follow the trend shown in the compilation performed by Török *et al.* [55].

Regarding the relative intensities, although there are not enough data to discern a trend, our results are of the same order of the few values available. Further experimental studies of the $K\alpha_5$ and $K\alpha_6$ transitions for different elements and induced by different excitation sources would be of interest in view of the scarcity of results about these lines.

E. $K\beta:K\alpha$ intensity ratios

Although the study of these ratios is not a main goal of this work, it is of interest to take advantage of the present measurements to compare the $K\beta:K\alpha$ intensity ratios with some of the experimental and theoretical data available in the literature. The $K\beta:K\alpha$ intensity ratios are plotted in Fig. 6. The $K\alpha$ and $K\beta$ intensities were taken from the spectra measured in this work and in a previous one [37], respectively. As can be seen, there is a good agreement between our results and the other experimental and theoretical values. It must be noted that there is no $K\beta$ diagram line for Mg in the dipole approximation; thus, the only contribution to the $K\beta$ intensity for this element comes from higher-order terms, particularly, from the $1s \rightarrow 3s$ decay.
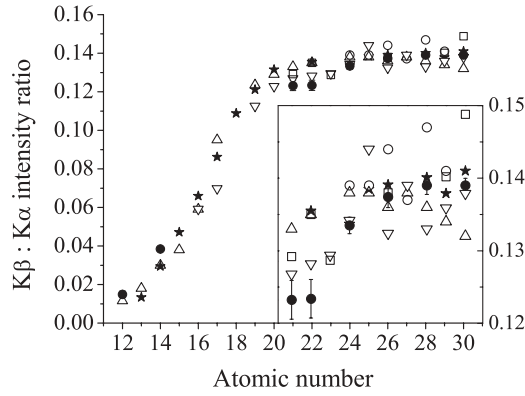
FIG. 6. $K\beta$:$K\alpha$ intensity ratio as a function of the atomic number. The point shape indicates the excitation source: electrons (circles), protons (squares), and photons (triangles). Filled circles: present results; open circles: [6]; squares: [39]; up triangles: [57], down triangles: [58]. Theoretical results given in [49] (stars) are also plotted. The inset shows an amplified view of the data for $21 \leqslant Z \leqslant 30$.

F. Influence of the incidence energy on the Si-$K\alpha$ satellite emission

As mentioned previously, the Si-$K\alpha$ satellite emission was studied at different incidence energies $E_o = 3, 6, 9, 12, 15$, and 18 keV. With this purpose, the spectral processing was carried out to obtain peak intensities imposing the normalization constraint explained in the beginning of Sec. III. All the line energies and natural widths were taken from the spectrum measured at 18 keV, for which the resolution and statistics were better. The relative intensities of the Si satellite lines are shown in Table V and Fig. 7. As can be seen from the table, a similar decreasing trend is observed from 6 keV for all the satellite lines, except for the $K\alpha_6$ and $K\alpha_{22}$ lines, which do not evidence any clear behavior. In addition, all the satellite transitions show an abrupt variation between 3 and 6 keV. In the particular case of the $K\alpha'$ line, it could not be distinguished from the background of the spectrum measured at 3 keV.

The intensity of the double-ionization satellite emission ($K\alpha' + K\alpha_3 + K\alpha_4$) relative to the $K\alpha$ group (disregarding triple and higher-order ionizations) is associated with the ratio between the double-ionization cross section σ_{KL} and the sum of the single- and double-ionization cross sections $\sigma_K + \sigma_{KL}$. Figure 7(a) presents this ratio obtained for Si as a function of the overvoltage (i.e., the incidence energy relative to the double-ionization threshold, E_o : E_{KL}), along

with experimental results given by Mauron and Dousse [29] for electron incidence on Al, Ca, and Co. This threshold is assumed to be $E_{KL}(Z) = E_K(Z) + E_{L3}(Z + 1)$, where E_K and E_{L3} are the K- and L_3-shell binding energies, respectively.

As can be seen, the double-ionization probability presents a significant increase from the threshold energy; and after reaching a maximum value, it slowly decreases, showing a behavior similar to the single-ionization cross section. Nevertheless, the maximum seems to move toward higher overvoltages for increasing atomic numbers. In addition, for any overvoltage, the double-ionization probability decreases with Z. The results presented here for Si follow the behavior exhibited by the values given in Ref. [29].

Results for the $K\alpha_{3,4}$ relative intensity obtained by photon incidence at different energies in Fe, Ni, and Zn by Kawatsura *et al.* [11] also show a similar behavior. Nevertheless the intensity ratios are lower than the results shown in Fig. 7(a), because the TS2 processes cannot take place with photon incidence.

In Fig. 7(b), the $K\alpha L^2$ (i.e., $K\alpha_{5,6}$) relative intensity is plotted as a function of the incidence energy. The values corresponding to $K\alpha L^1$ are also shown for comparison. It can be easily observed that the intensity of the $K\alpha L^2$ lines behaves in the same way as the corresponding $K\alpha L^1$ ones, but one order of magnitude lower, because the triple-ionization processes are less probable than double-ionization events.

IV. CONCLUSION

The emission of $K\alpha$ satellite lines in atomic relaxation processes of eight elements in the range of $12 \leqslant Z \leqslant 30$ was studied by means of electron incidence and wavelength dispersive x-ray spectroscopy. Energy shifts and relative transition probabilities of the $K\alpha_{22}$, $K\alpha_{12}$, $K\alpha'$, $K\alpha_3$, $K\alpha_4$, $K\alpha_5$, and $K\alpha_6$ lines were determined through a careful spectral processing.

The results presented here agree with the general trends observed by other authors, i.e., all the satellite lines associated with $2p$ spectator-hole transitions exhibit an increase in the energy shift and a decrease on the relative intensity as a function of the atomic number.

The $K\alpha_{12}$ and $K\alpha_{22}$ structures represent a significant fraction of the diagram $K\alpha_1$ and $K\alpha_2$ lines (above 30%) for $3d$ transition elements. The theoretical calculations of electron shake probabilities are below the experimental

TABLE V. Relative probabilities of the Si-$K\alpha$ satellite transitions with respect to the whole $K\alpha$ group at different incidence energies. Numbers in parentheses represent the estimated uncertainties in the last digit.

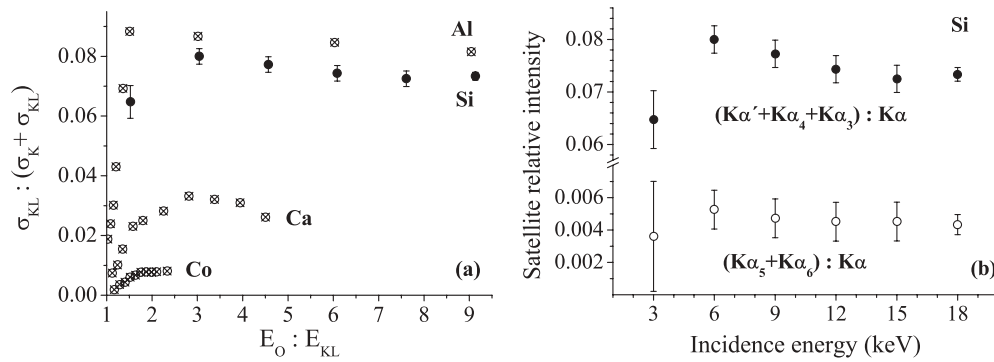| Transition	Incidence energy					
	3 keV	6 keV	9 keV	12 keV	15 keV	18 keV
$K\alpha_{22}$	0.17(4)	0.19(2)	0.19(2)	0.19(2)	0.19(2)	0.178(7)
$K\alpha'$		0.0027(6)	0.0023(6)	0.0022(6)	0.0022(6)	0.0017(3)
$K\alpha_3$	0.052(4)	0.063(2)	0.059(2)	0.057(2)	0.055(2)	0.0547(9)
$K\alpha_4$	0.013(4)	0.017(2)	0.018(2)	0.018(2)	0.017(2)	0.0170(9)
$K\alpha_5$	0.001(2)	0.0027(8)	0.0025(8)	0.0023(8)	0.0023(8)	0.0022(4)
$K\alpha_6$	0.002(3)	0.003(1)	0.002(1)	0.002(1)	0.002(1)	0.0022(5)

FIG. 7. Satellite emission as a function of the incidence energy. (a) Double-ionization cross section relative to the sum of single- and double-ionization cross sections as a function of the incidence energy normalized by the double-excitation threshold. Filled circles: present results; crossed circles: [29]. (b) Satellite emission intensity relative to the $K\alpha$ group obtained in this work as a function of the incidence energy for silicon. Open circles: triple-ionization lines ($K\alpha_5 + K\alpha_6$); filled circles: double-ionization lines ($K\alpha' + K\alpha_3 + K\alpha_4$).

results. This difference could be attributed to the energy spread of the multiplet corresponding to the involved transitions.

From the good agreement between the values of $K\alpha_{3,4}$ relative intensities obtained by electron and photon incidence, and their comparison with theoretical calculations of shake probabilities, it can be concluded that, even when these processes are important mechanisms for the creation of multiple vacancies, TS1 processes also contribute to the $K\alpha_{3,4}$ emission, whereas TS2 mechanisms are of less importance in the case of electron incidence. From the comparison with results obtained by proton impact, it can also be concluded that the ratio between the probabilities of double-vacancy creation by protons and by electrons is the same (around 1.5) for elements with atomic numbers ranging from 12 to 30. On the other hand, the behavior of the data available obtained by heavy-ion incidence suggests that other processes are involved in the creation of spectator holes.

The study carried out about the emission of Si satellite lines induced by electrons with different incidence energies produced results that are in agreement with the behavior observed in similar studies carried out for other elements. Finally, it can be stated that the $K\alpha L^2$ intensities have a similar behavior to the $K\alpha L^1$ ones, although one order of magnitude lower, due to the lower probability of triple ionization.

[1] C. H. Shaw and L. G. Parratt, Phys. Rev. **50**, 1006 (1936).

[2] G. Graeffe, H. Juslén, and M. Karras, J. Phys. B **10**, 3219 (1977).

[3] P. Chevallier, M. Tavernier, and J. P. Briand, J. Phys. B **11**, L171 (1978).

[4] G. R. Babu, V. Gopalakrishna, M. N. L. Raju, K. Parthasaradhi, V. R. K. Murty, M. V. R. Murti, and K. S. Rao, Phys. Rev. A **36**, 386 (1987).

[5] H. Sorum, J. Phys. F **17**, 417 (1987).

[6] G. Hölzer, M. Fritsch, M. Deutsch, J. Härtwig, and E. Förster, Phys. Rev. A **56**, 4554 (1997).

[7] M. Fritsch, C. C. Kao, K. Hämäläinen, O. Gang, E. Förster, and M. Deutsch, Phys. Rev. A **57**, 1686 (1998).

[8] D. F. Anagnostopoulos, R. Sharon, D. Gotta, and M. Deutsch, Phys. Rev. A **60**, 2018 (1999).

[9] H. Verma, J. Phys. B **33**, 3407 (2000).

[10] O. Mauron, J.-Cl. Dousse, J. Hoszowska, J. P. Marques, F. Parente, and M. Polasik, Phys. Rev. A **62**, 062508 (2000).

[11] K. Kawatsura, T. Morikawa, K. Takahiro, M. Oura, H. Yamaoka, K. Maeda, S. Hayakawa, S. Ito, M. Terasawa, and T. Mukoyama, J. Phys. B **36**, 4065 (2003).

[12] N. Shigeoka, H. Oohashi, T. Tochio, Y. Ito, T. Mukoyama, A. M. Vlaicu, and S. Fukushima, Phys. Rev. A **69**, 052505 (2004).

[13] M. Deutsch, E. Förster, G. Hölzer, J. Härtwig, K. Hämäläinen, C.-C. Kao, S. Huotari, and R. Diamant, J. Res. Nat. Inst. Stand. Technol. **109**, 75 (2004).

[14] K. Yokoi, H. Oohashi, Y. Ito, T. Tochio, and T. Shoji, Radiat. Phys. Chem. **75**, 1461 (2006).

[15] R. Diamant, S. Huotari, K. Hämäläinen, R. Sharon, C. C. Kao, and M. Deutsch, Radiat. Phys. Chem. **75**, 1434 (2006).

[16] Y. Ito, T. Tochio, H. Oohashi, and A. M. Vlaicu, Radiat. Phys. Chem. **75**, 1534 (2006).

[17] B. Hodge, R. Kauffman, C. F. Moore, and P. Richard, J. Phys. B **6**, 2468 (1973).

[18] M. Kavičič, M. Budnar, A. Mühleisen, and I. Török, Nucl. Instrum. Methods B **136–138**, 173 (1998).

[19] M. Kavičič, Phys. Rev. A **68**, 022713 (2003).

[20] M. Kavičič, A. G. Karydas, and Ch. Zarkadas, Nucl. Instrum. Methods B **222**, 601 (2004).

[21] K. A. Jamison, C. W. Woods, R. L. Kauffman, and P. Richard, Phys. Rev. A **11**, 505 (1975).

[22] K. A. Jamison, J. M. Hall, J. Oltjen, C. W. Woods, R. L. Kauffman, T. J. Gray, and P. Richard, Phys. Rev. A **14**, 937 (1976).

[23] L. G. Parratt, Phys. Rev. **49**, 502 (1936).

[24] L. G. Parratt, Phys. Rev. **50**, 1 (1936).

[25] D. W. Fischer and W. L. Baun, J. Appl. Phys. **36**, 534 (1965).
[26] U. D. Misra and L. M. Watson, Phys. Scr. **36**, 673 (1987).
[27] S. I. Salem and B. L. Scott, Phys. Rev. A **35**, 1607 (1987).
[28] N. Maskil and M. Deutsch, Phys. Rev. A **38**, 3467 (1988).
[29] O. Mauron and J.-Cl. Dousse, Phys. Rev. A **66**, 042713 (2002).
[30] F. A. Gianturco, J. Phys. B (Proc. Phys. Soc.) **1**, 614 (1968).
[31] B. Hodge, Phys. Rev. A **16**, 1543 (1977).
[32] M. Deutsch, J. Phys. B **20**, L681 (1987).
[33] M. Deutsch, Phys. Rev. A **39**, 1077 (1989).
[34] M. Deutsch, Phys. Rev. A **39**, 3956 (1989).
[35] J. Kawai, Y. Nihei, Y. Z. Bai, K. Fujisawa, and Y. Gohshi, Phys. Rev. A **39**, 3686 (1989).
[36] T. K. Mukherjee and P. K. Mukherjee, Phys. Scr. **59**, 219 (1999).
[37] S. P. Limandri, A. C. Carreras, R. D. Bonetto, and J. C. Trincavelli, Phys. Rev. A **81**, 012504 (2010).
[38] S. P. Limandri, J. C. Trincavelli, R. D. Bonetto, and A. C. Carreras, Phys. Rev. A **78**, 022518 (2008).
[39] S. J. Cipolla, Nucl. Instrum. Methods A **422**, 546 (1999).
[40] Ch. Herren and J.-Cl. Dousse, Phys. Rev. A **56**, 2750 (1997).
[41] I. Török and T. Bondár, Nucl. Instrum. Methods B **154**, 272 (1999).
[42] R. Bonetto, G. Castellano, and J. Trincavelli, X-Ray Spectrom. **30**, 313 (2001).
[43] R. D. Bonetto, A. C. Carreras, J. Trincavelli, and G. Castellano, J. Phys. B **37**, 1477 (2004).
[44] S. P. Limandri, R. D. Bonetto, H. O. Di Rocco, and J. C. Trincavelli, Spectrochim. Acta B **63**, 962 (2008).
[45] J. Trincavelli and G. Castellano, Spectrochim. Acta B **63**, 1 (2008).
[46] J. Trincavelli, S. Limandri, A. Carreras, and R. Bonetto, Microsc. Microanal. **14**, 306 (2008).
[47] J. L. Campbell and T. Papp, At. Data Nucl. Data Tables **77**, 1 (2001).
[48] J. A. Bearden, Rev. Mod. Phys. **39**, 78 (1967).
[49] J. H. Scofield, Phys. Rev. A **9**, 1041 (1974).
[50] A. N. Nigam and S. N. Soni, J. Phys. C **13**, 1567 (1980).
[51] S. Galambosi, H. Sutinen, A. Mattila, K. Hämäläinen, R. Sharon, C. C. Kao, and M. Deutsch, Phys. Rev. A **67**, 022510 (2003).
[52] M. Deutsch, G. Hölzer, J. Härtwig, J. Wolf, M. Fritsch, and E. Förster, Phys. Rev. A **51**, 283 (1995).
[53] T. Mukoyama and K. Taniguchi, Phys. Rev. A **36**, 693 (1987).
[54] O. Keski-Rahkonen, E. Mikkola, K. Reinikainen, and M. Lehkonen, J. Phys. C **18**, 2961 (1985).
[55] I. Török, T. Papp, and S. Raman, Nucl. Instrum. Methods B **150**, 8 (1999).
[56] A. R. Knudson, D. J. Nagel, P. G. Burkhalter, and K. L. Dunning, Phys. Rev. Lett. **26**, 1149 (1971).
[57] S. I. Salem, T. H. Falconer, and R. W. Winchell, Phys. Rev. A **6**, 2147 (1972).
[58] B. Ertuğral, G. Apaydın, U. Çevik, M. Ertuğrul, and A.İ. Kobya, Radiat. Phys. Chem. **76**, 15 (2007).